Electron Transfer Across Modular Oligo-p-phenylene Bridges in Ru(bpy)(2)(bpy-ph(n)-DQ)(4+) (n=1-5) Dyads. Unusual Effects of Bridge Elongation

ARTICLE *in* THE JOURNAL OF PHYSICAL CHEMISTRY A · NOVEMBER 2011

Impact Factor: 2.69 · DOI: 10.1021/jp209858p · Source: PubMed

THE JOURNAL OF PHYSICAL CHEMISTRY A

ARTICLE

pubs.acs.org/JPCA

Electron Transfer Across Modular Oligo-*p*-phenylene Bridges in $Ru(bpy)_2(bpy-ph_n-DQ)^{4+}$ ($n = 1-5$) Dyads. Unusual Effects of Bridge Elongation

Maria Teresa Indelli,[†,‡] Michele Orlandi,[†,▼] Claudio Chiorboli,[§] Marcella Ravaglia,[†,∥] Franco Scandola,*[,†,‡] Frederic Lafolet,[▽] Steve Welter,[△] and Luisa De Cola*[,⊥]

[†]Dipartimento di Chimica, Università di Ferrara, and Centro Interuniversitario per la Conversione Chimica dell'Energia Solare (SolarChem), sezione di Ferrara, 44100 Ferrara, Italy

[‡]INSTM, Sezione di Ferrara, 44100 Ferrara, Italy

[§]ISOF-CNR, Sezione di Ferrara, 44100 Ferrara, Italy

[⊥]Westfälische Wilhelms-Universität Münster, Physikalisches Institut, Mendelstrasse 7, 48149 Münster, Germany, and Center for Nanotechnology (CeNTech), Heisenbergstrasse 11, 48149 Münster, Germany

Supporting Information

ABSTRACT: A series of dyads of general formula $Ru(bpy)_2(bpy-ph_n-DQ)^{4+}$ ($n = 1-5$), based on a Ru(II) polypyridine unit as photoexcitable donor, a set of oligo-*p*-phenylene bridges with 1−5 modular units, and a cyclo-diquaternarized 2,2′-bipyridine (DQ^{2+}) as electron acceptor unit, have been synthesized. Their spectroscopic and photophysical properties have been investigated in CH_3CN and CH_2Cl_2 by time-resolved emission and absorption spectroscopy in the nanosecond and picosecond time scale. The experimental study has also been complemented with a computational investigation carried out on the whole series of dyads. The absorption spectra of the dyads show new spectroscopic transitions, in addition to those characteristic of the donor, bridge, and acceptor fragments. DFT calculations suggest the assignment of such bands as bridge-to-acceptor (π ph_n) → (π^* DQ) charge-transfer transitions. This assignment is consistent with the solvatochromic and spectroelectrochemical behavior of the new bands. For all the dyads at room temperature in fluid solution, the typical ^{3}MLCT luminescence of the Ru(II) polypyridine unit is strongly (>90%) quenched, supporting the occurrence of an efficient intramolecular photoinduced electron transfer. The study has revealed, however, that the photophysical mechanism is actually more complex than presumed on the basis of a simple photoinduced electron-transfer scheme. For $n = 1$, very fast (few picoseconds) photoinduced electron transfer from the MLCT state localized on the substituted bpy ligand to the DQ unit has been observed, followed by slower interligand hopping and charge recombination. For $n = 2-5$, MLCT excited-state quenching takes place without transient detection of charge-separated product, indicating that charge recombination is faster than charge separation. This behavior can be rationalized in terms of the superexchange couplings expected through this type of bridges for the two processes. The kinetics of MLCT quenching in the dyads with $n = 1-5$ does not follow the usual exponential falloff with bridge length: after a regular decrease for $n = 1-3$, the rate constants become almost insensitive to bridge length for $n = 3-5$. The rationale of this uncommon behavior, as suggested by DFT calculations, lies in a switch in the MLCT quenching mechanism with increasing bridge length, from oxidative quenching by the DQ acceptor to reductive quenching by the bridge.

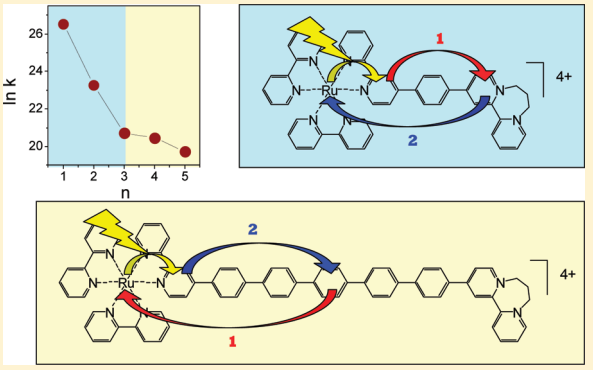

INTRODUCTION

Driven by potential applications in the fields of artificial photosynthesis,[1] molecular electronics, and photonics,[2] the study of charge transport from donor to acceptor units across molecular bridges is a subject of continuing interest.[3] In this context, the bridges are often designated as *molecular wires*, despite the fact that their behavior is generally quite far from that of a conventional ohmic-type conductor. In fact, for many experimental cases involving saturated or partially unsaturated organic bridges, the energy levels of the wires investigated are far apart from those of the donor and acceptor sites, so that the electron has to tunnel in a single coherent step from donor to acceptor, without being localized at any time on the "wire". Nevertheless, the nature of the bridge plays an important role in determining the electron-transfer rates.

Electron transfer in a donor−bridge−acceptor (D−B−A) system (Figure 1) can be described by standard nonadiabatic electron transfer theory,[4] where the transfer probability is

Received: October 13, 2011
Revised: November 21, 2011
Published: November 22, 2011

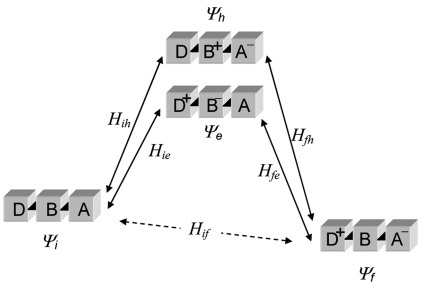

Figure 1. Schematic representation of superexchange in a donor−bridge−acceptor system. The donor−acceptor electronic coupling is mediated by interaction of initial (D−B−A) and final (D^+−B−A^-) states with bridge-localized virtual states of electron- (D^+−B^-−A) and hole-transfer (D−B^+−A^-) type.

given by

$$k = \frac{4\pi}{h} H_{if}{}^2 \mathrm{FCWD} \quad (1)$$

where H_{if} is the electronic matrix element between the initial and final states of the process (donor−acceptor electronic coupling) and FCWD is a nuclear factor (Franck−Condon weighted density of states) accounting for the combined effects of driving force and reorganizational energy. The role of the bridge as mediator of the donor−acceptor electronic coupling can be conveniently described in terms of *superexchange*,[3,5] as second-order interaction of the initial and final states via high-energy charge transfer "virtual" states involving the bridge.

In this formalism, the electronic coupling H_{if} between the initial (D−B−A) and final (D^+−B−A^-) states is given by

$$H_{if} = \frac{H_{ie}H_{fe}}{\Delta E_e} + \frac{H_{ih}H_{fh}}{\Delta E_h} \quad (2)$$

where H_{ie}, H_{fe}, H_{ih}, H_{fh} are the couplings between the initial/final states and the bridge-localized electron-transfer (D^+−B^-−A) and hole-transfer (D−B^+−A^-) virtual states, and ΔE_e and ΔE_h are the energy differences between the virtual states and the initial/final levels (taken at the transition-state nuclear geometry, where the initial and final state have the same energy). The same model can be applied to modular bridges involving a number (n) of repeating units. In such a case, each term in eq 2 takes the form

$$H_{if} = \frac{H_i H_f}{\Delta E}\left(\frac{H_{mn}}{\Delta E}\right)^{n-1} \quad (3)$$

where H_i and H_f are the couplings between the initial/final states and the virtual states localized on the bridge subunits adjacent to the donor and acceptor, while H_{mn} is the coupling between adjacent subunits of the bridge, and ΔE is the energy difference between the virtual states of the bridge and the initial/final state (at the transition-state nuclear geometry), ideally assumed to be independent of the bridge length. This translates into an exponential dependence on the number of modular units in the bridge, i.e., on donor−acceptor distance r_{AB}

$$H_{if} = H_{if}(0) \exp\left[-\frac{\beta}{2}(r_{AB} - r_0)\right] \quad (4)$$

In eq 4, r_0 and $H_{if}(0)$ represent the donor−acceptor distance and electronic coupling for a single-module bridge, and $\beta = (2/r_m)\ln(\Delta E/H_{mn})$ (where r_m is the length of an individual module) is the attenuation factor of the electron-transfer rate with distance. The β factor depends on the intermodule couplings within the bridge and is often considered as a parameter that quantifies the intrinsic ability of the bridge to promote long-distance electron transfer (the lower β, the higher the "conductivity" of the "molecular wire"). It should be noticed, however, that β is not entirely bridge-specific, as it also depends on the energy gap between the bridge-localized virtual states and the initial/final state,[3d] and thus also on the donor and acceptor units involved.[6] These superexchange models have been extensively tested with studies of *photoinduced electron transfer* in donor−bridge−acceptor systems ("dyads") where the process can be triggered by electronic excitation of either the donor or the acceptor. In particular, the predicted exponential decay of the rates with distance has been often verified in homogeneous series of dyads containing modular organic bridges of variable length.[3]

Exceptions to this general behavior have been observed with highly conjugated organic bridges, when the bridge-localized electron/hole-transfer states may become lower in energy than the electronically excited state. In such cases, injection of electrons (or holes) into the wire can occur and the process (charge "hopping" or "transport"[3a]) has an inverse dependence on a small power (1−2) of distance, more similar to conventional ohmic conduction. Interesting examples of switch from superexchange to electron injection[7] or hole injection[8] upon bridge elongation have been reported by Wasielewski and co-workers.

Because of their modular nature and longitudinal rigidity, an interesting class of molecular bridges is that of oligo-*p*-phenylenes. Although the individual units have fully aromatic π systems, extensive delocalization along the oligomeric chain is prevented by nonbonded interactions that force adjacent units in a twisted geometry (ca. 40° angle in the gas phase[9]). Onuchich and Beratan[10] first considered electron transfer through biphenyl spacers from a theoretical viewpoint. In pioneering experimental work by McLendon and co-workers[11] on bis-porphyrin systems with oligo-*p*-phenylene spacers, a sevenfold attenuation in photoinduced electron-transfer rate was obtained for each additional *p*-phenylene unit (β = 0.4 $Å^{-1}$).[11b] Extensive work has recently been performed by Wasielewski and co-workers[8,12] on oligo-*p*-phenylene bridged dyads where a perylenebisimide acts as a photoexcited acceptor and a phenothiazine as the electron donor quencher. Inorganic dyads with oligo-*p*-phenylene spacers have also been investigated. The extensive series of dyads developed by Sauvage and co-workers[13] and by De Cola and co-workers,[14,15] involving polypyridyl complexes of Ru(II), Os(II), and Ir(III) as donor/acceptor units, were designed for the study of *energy* (rather than electron) transfer. Recently, we have investigated bimetallic dyads involving Ru(II) polypyridine units as photoexcited donor and a Rh(III) unit as electron acceptor.[16] Despite some limitations (small driving force, limited number of modular spacers) the study of photoinduced electron transfer in these dyads gave interesting information on the β attenuation factor and on the effect of intermodule twist angle on rates. Wegner has recently reviewed the effect of the donor−bridge−acceptor energetics on the distance dependence of electron transfer across modular bridges, including oligo *p*-xylene bridges.[17]

In this work, we set out to synthesize and study a series of dyads (Scheme 1) based on a Ru(II) polypyridine unit as photoexcitable donor, a set of oligo-*p*-phenylene bridges with 1−5 modular units, and a cyclo-diquaternarized bipyridine (DQ^{2+}) as electron acceptor unit. In this series, the long lifetime of the donor excited state and the favorable driving force are appropriate, in principle, to obtain efficient long-range photoinduced electron transfer. As it

Scheme 1

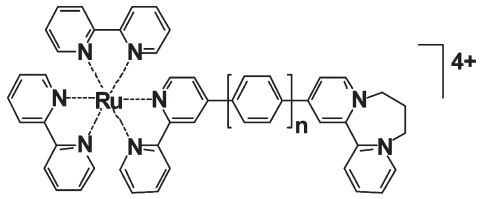

$Ru(bpy)_2(bpy\text{-}ph_n\text{-}DQ)^{4+}$ n = 1-5

will be seen, the study has revealed that the behavior of this type of bridges is actually much more complex than presumed on the basis of the above simple superexchange mechanism. To help in the interpretation of this intriguing behavior, a DFT computational investigation has also been carried out on the series of dyads.

EXPERIMENTAL SECTION

Materials. For photophysical measurements spectroscopic grade organic solvents (Merck Uvasol) were used without further purification. Other chemicals were all of reagent grade quality.

Silica Gel (Merck) used in chromatographic purification was 200−400 mesh.

Syntheses. The series of nonquaternarized $Ru(bpy)_2(bpy-ph_n-bpy)^{2+}$ ($n = 1-5$) complexes, used in this work as chemical precursors and as model compounds, was available from previous work.[15,16]

The syntheses of the dyads were carried out starting from the appropriate $Ru(bpy)_2(bpy-ph_n-bpy)^{2+}$ complex by cycloquaternarization of the free bipyridyl group of the bridging ligand. The same general procedure was followed for all the compounds with minor changes concerning the volume of the reaction mixture. A typical synthesis is described below for $Ru(bpy)_2(bpy-ph_2-DQ)^{4+}$. All the compounds were isolated as PF_6^- salts and identified (see data below) by ^{1}H NMR (400 MHz, CD_3CN) and mass spectroscopy (electron spray ionization, CH_3CN matrix). The ^{1}H NMR spectrum of $Ru(bpy)_2(bpy-ph_2-DQ)^{4+}$ is reported as an example in the Supporting Information (Figure S1).

$Ru(bpy)_2(bpy-ph_2-DQ)^{4+}$. A 116 mg (0.25 mmol) amount of $[Ru(bpy)_2(bpy-ph_n-bpy)](PF_6)_2$ was added to 25 mL of hot 1,3 dibromopropane and stirred in argon atmosphere for 15 min. The reaction mixture was then heated for 72 h at ca. 110 °C under continuous stirring. After cooling at room temperature, the solvent was evaporated and acetonitrile and $NaPF_6$ were added. The hexafluorophosphate salt was precipitated by addition of water and evaporation of acetonitrile. The crude product was washed with water, dissolved in a minimum of acetonitrile, and purified by column chromatography on silica gel using MeCN/MeOH/H_2O/saturated aqueous KNO_3, 40/10/10/1 as eluent. Elution was first performed to collect the unreacted $[Ru(bpy)_2(bpy-ph_2-bpy)](PF_6)_2$. Then elution was continued until the main fraction containing the desired product was completely eluted, leaving a small fraction containing unidentified byproducts at the top of the column. The fraction containing the pure product was concentrated to 2 mL, and solid NH_4PF_6 was added. The product was isolated by filtration, washed extensively with water, and dried under vacuum. Purity was verified by TLC (silica gel, MeCN/MeOH/H_2O/saturated aqueous KNO_3, 40/10/10/1 as eluent). (Yield 60%.)

$Ru(bpy)_2(bpy-ph-DQ)^{4+}$. ^{1}H NMR (400 MHz, CD_3CN) δ 9.08 (d, 1H, J = 5.76 Hz), 9.04 (m, 1H), 8.93 (t, 1H, J = 9.5 Hz), 8.87 (bs, 1H), 8.76 (d, 1H, J = 10.5 Hz), 8.67 (m, 2H), 8.56 (m, 5H), 8.43 (t, 1H, J = 9.5 Hz), 8.22 (d, 2H, J = 11.4 Hz), 8.28 (d, 2H, J = 14.4 Hz), 8.13 (m, 5H), 7.83 (m, 7H), 7.48 (m, 5H), 4.95 (m, 2H), 4.48 (m, 2H), 2.95 (m, 2H). MS (ESI) m/z 221.0 ($[M-CH_3CN]^{4+}/4$ requires m/z 221.4).

$Ru(bpy)_2(bpy-ph_2-DQ)^{4+}$. ^{1}H NMR (400 MHz, CD_3CN) δ 9.08 (d, 1H, J = 5.76 Hz), 9.04 (m, 1H), 8.93 (t, 1H, J = 9.5 Hz), 8.86 (bs, 1H), 8.77 (d, 1H, J = 10.5 Hz), 8.67 (m, 2H), 8.56 (m, 5H), 8.43 (t, 1H, J = 9.5 Hz), 8.23 (d, 2H, J = 11.4 Hz), 8.12 (m, 11 H), 7.82 (m, 7H), 7.48 (m, 5H), 4.95 (m, 2H), 4.48 (m, 2H), 2.95 (m, 2H). MS (ESI) m/z 229.9 ($[M]^{4+}/4$ requires m/z 230.11), m/z 240.2 ($[M-CH_3CN]^{4+}/4$ requires m/z 240.3).

$Ru(bpy)_2(bpy-ph_3-DQ)^{4+}$. ^{1}H NMR (400 MHz, CD_3CN) δ 9.10 (d, 1H, J = 5.76 Hz), 9.03 (m, 1H), 8.93 (t, 1H, J = 9.5 Hz), 8.86 (bs, 1H), 8.78 (d, 1H, J = 10.5 Hz), 8.68 (m, 2H), 8.58 (m, 5H), 8.43 (t, 1H, J = 9.5 Hz), 8.24 (d, 2H, J = 11.4 Hz), 8.10 (m, 15H), 7.82 (m, 7H), 7.48 (m, 5H), 4.95 (m, 2H), 4.48 (m, 2H), 2.95 (m, 2H). MS (ESI) m/z 248.9 ($[M]^{4+}/4$ requires m/z 249.1).

$Ru(bpy)_2(bpy-ph_4-DQ)^{4+}$. ^{1}H NMR(400 MHz, CD_3CN) δ 9.10 (d, 1H, J = 5.76 Hz), 9.02 (m, 1H), 8.92 (t, 1H, J = 9.5 Hz), 8.85 (bs, 1H), 8.76 (d, 1H, J = 10.5 Hz), 8.68 (m, 2H), 8.57 (m, 5H), 8.45 (t, 1H, J = 9.5 Hz), 8.23 (m, 2H), 8.10 (m, 19H), 7.82 (m, 7H), 7.47 (m, 5H), 4.95 (m, 2H), 4.48 (m, 2H), 2.95 (m, 2H). MS (ESI) m/z 267.9 ($[M]^{4+}/4$ requires m/z 268.1).

$Ru(bpy)_2(bpy-ph_5-DQ)^{4+}$. ^{1}H NMR(400 MHz, CD_3CN) δ 9.08 (d, 1H, J = 5.76 Hz), 9.00 (m, 1H), 8.92 (t, 1H, J = 9.5 Hz), 8.85 (bs, 1H), 8.76 (d, 1H, J = 10.5 Hz), 8.67 (m, 2H), 8.57 (m, 5H), 8.43 (t, 1H, J = 9.5 Hz), 8.22 (d, 2H, J = 11.4 Hz), 8.10 (m, 23H), 7.82 (m, 7H), 7.47 (m, 5H), 4.95 (m, 2H), 4.48 (m, 2H), 2.95 (m, 2H). MS (ESI) m/z 287.0 ($[M]^{4+}/4$ requires m/z 287.1).

Apparatus and Procedures. ^{1}H NMR spectra were recorded in CD_3Cl on a Varian Mercury spectrometer (400 MHz) with residual nondeuterated solvent signal as reference .Electron spray ionization (ESI) mass spectra were measured with a Micromass ZMD2000 spectrometer.

UV−vis spectra were recorded with a Perkin-Elmer LAMDA40 spectrophotometer. Luminescence spectra were taken on a Spex Fluoromax-2 equipped with Hamamatsu R928 tubes.

Emission lifetimes were measured by time-correlated single-photon counting technique, using a TCSPC apparatus (PicoQuant Picoharp 300), equipped with subnanosecond LED sources (280−600 nm range, 300−700 ps pulse width) powered with a PicoQuant PDL 800-B variable (2.5−40 MHz) pulsed power supply. The experiments were performed using 460 nm LED (300 ps pulse width) as excitation source. The decays were analyzed by means of PicoQuant FluoFit Global Fluorescence Decay Analysis software. The time resolution of the system after the deconvolution procedure is 250 ps, and estimated errors are 10% for lifetime values.

Femtosecond time-resolved experiments were performed using a pump−probe setup[18] based on the Spectra-Physics Hurricane Ti:sapphire laser source and the Ultrafast Systems Helios spectrometer. The 560 nm pump pulses were generated with a Spectra Physics 800 OPA. Probe pulses were obtained by continuum generation on a sapphire plate (useful spectral range: 450−800 nm). Effective time resolution ca. 300 fs, temporal chirp over the white-light 450−750 nm range ca. 200 fs, temporal window of the optical delay stage 0−1000 ps. The time-resolved spectral data were analyzed with the Ultrafast Systems Surface Explorer Pro software.

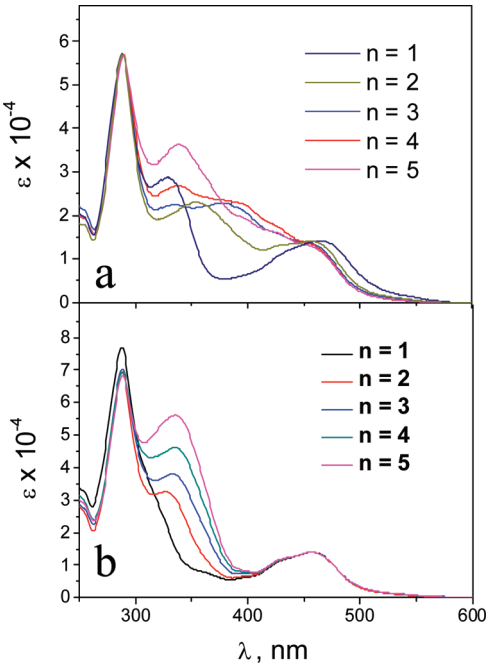

Figure 2. Absorption spectra of the $Ru(bpy)_2(bpy-ph_n-DQ)^{4+}$ dyads (a) and of the $Ru(bpy)_2(bpy-ph_n-bpy)^{2+}$ model complexes (b) in CH_3CN solution at room temperature.

Nanosecond transient absorption measurements were performed with an Applied Photophysics laser flash photolysis apparatus, using a frequency-doubled (532 nm, 330 mJ) or tripled (355 nm, 160 mJ) Surelite Continuum II Nd/YAG laser (half-width 6−8 ns) as excitation source. Transient detection using photomultiplier−oscilloscope combination (Hamamatsu R928, LeCroy 9360) or gated intensified CCD-Camera (Princeton Instruments PI-MAX II, with Acton SpectraPro 2300i triple grating flat field monochromator, RB GenII intensifier, ST133 controller, and a PTG pulser).

Cyclic voltammetric measurements were carried out with a PC-interfaced Eco Chemie Autolab/Pgstat30 Potentiostat. Argon-purged solutions in CH_2Cl_2 and CH_3CN (Romil, Hi-dry) containing 0.1 M $TBAPF_6$ (Fluka, electrochemical grade; dried in an oven) were used. A conventional three-electrode cell assembly was used. A saturated calomel electrode (SCE, 6 mm^2 AMEL) and a platinum wire were used as reference and counter electrodes, respectively; a glassy carbon electrode (8 mm^2, AMEL) was used as a working electrode. The scan rate was 200 mV/s.

Spectroelectrochemistry measurements were performed in CH_3CN, using an optically transparent thin layer electrochemical (OTTLE) cell (optical path 1 mm, platinum mini-grid working electrode, platinum wire as counter electrode, silver wire as quasi-reference electrode, 0.1 M $(TBA)PF_6$ electrolyte).

Computational Techniques. Ground-state and lowest triplet-state geometries have been optimized at the DFT level of theory, using the B3LYP hybrid functional or the unrestricted version uB3LYP for triplet. The 6-31G* basis set has been employed for all elements except Ru, for which LANL2DZ has been used. Energies, molecular orbitals, and singly occupied molecular orbitals in the case of triplet have been calculated at the same level of theory and with the same basis set used for geometry optimization. Solvents have been modeled with the polarizable continuum model. All calculations have been performed with the Gaussian 2003 software package.[19]

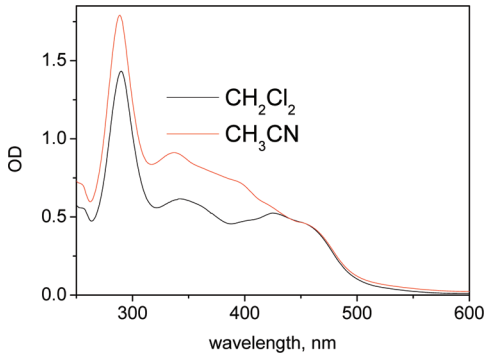

Figure 3. Solvatochromic behavior of the $Ru(bpy)_2(bpy-ph_4-DQ)^{4+}$ dyad.

Table 1. Redox Potentials of the $[Ru-ph_n-DQ]^{4+}$ Dyads (n = 1, 4) in CH_3CN[a]

	$E_{1/2}$ (V)		
	oxidation	reduction	
compound	Ru(II/III)	$DQ^{2+/+}$	$DQ^{+/0}$
$Ru(bpy)_2(bpy-ph-DQ)^{4+}$	+1.26	−0.54	−0.84
$Ru(bpy)_2(bpy-ph_4-DQ)^{4+}$	+1.29	−0.52	−0.83
$bpy-ph-DQ^{2+}$		−0.61	−0.93

[a] CH_3CN solution with 0.1 M $TBAPF_6$; reversible waves, $E_p^a - E_p^c$ = ca. 60 mV; potential values vs SCE.

RESULTS

Absorption Spectra. The absorption spectra of the $Ru(bpy)_2(bpy-ph_n-DQ)^{4+}$ dyads in acetonitrile solution are shown in Figure 2a. The spectra of the $Ru(bpy)_2(bpy-ph_n-bpy)^{2+}$ nonquaternarized complexes, employed as model compounds for the donor unit of the dyads, are also shown for comparison (Figure 2b).

The absorption spectra of the dyads were also measured in CH_2Cl_2 solutions. Going from CH_3CN to CH_2Cl_2, significant spectral changes in the 350−450 region are observed, especially for the dyads with $n > 2$. The absorption spectrum of $Ru(bpy)_2(bpy-ph_4-DQ)^{4+}$ in CH_3CN and in CH_2Cl_2 is reported in Figure 3. The corresponding nonquaternarized model compounds do not show any significant solvatochromism.

Redox Behavior. The electrochemical behavior of the dyads was studied by cyclic voltammetry in acetonitrile solution ($TBAPF_6$ 0.1 M supporting electrolyte, glassy carbon working electrode, SCE reference electrode, platinum counter electrode). For purposes of comparison, the electrochemical behavior of the free $bpy-ph-DQ^{2+}$ ligand was studied under the same experimental conditions. All the dyads exhibit the same behavior regardless of the number of phenylene spacers. The anodic region (0.0, + 1.5 V vs SCE) is characterized by a reversible oxidation wave, due to oxidation of the Ru(II) center. In the cathodic region (0.0, −1.2 V vs SCE), two subsequent well-resolved reversible reduction waves are observed. By comparison with the $bpy-ph-DQ^{2+}$ ligand, these waves are easily assigned to the reduction of the quaternarized bipyridine unit and are almost unaffected by the number of phenylene units, as exemplified by the results for n = 1 and n = 4 reported in Table 1.

Spectroelectrochemical measurements were performed in CH_3CN to obtain the absorption spectrum of the reduced forms

dx.doi.org/10.1021/jp209858p | J. Phys. Chem. A 2012, 116, 119–131

Table 2. Photophysical Data for Dyads $Ru(bpy)_2(bpy-ph_n-DQ)^{4+}$ (n = 1−5)

	τ_{em}, ns[a]		τ_{abs}, ns[b]		k_{el}, s^{-1} [e]	
dyad	CH_3CN	CH_2Cl_2	CH_3CN	CH_2Cl_2	CH_3CN	CH_2Cl_2
$Ru(bpy)_2(bpy-ph-DQ)^{4+}$	<0. 25	<0.25	<0.001[c]	0.002[d]	$>1.0 \times 10^{12}$	5.0×10^{11}
$Ru(bpy)_2(bpy-ph_2-DQ)^{4+}$	<0.25	0.76	0.080	0.680	1.2×10^{10}	1.4×10^{9}
$Ru(bpy)_2(bpy-ph_3-DQ)^{4+}$	1.00	3.20	1.0	>2.0	1.0×10^{9}	3.1×10^{8}
$Ru(bpy)_2(bpy-ph_4-DQ)^{4+}$	1.24	1.36	∼1.5	>2.0	8.1×10^{8}	7.3×10^{8}
$Ru(bpy)_2(bpy-ph_5-DQ)^{4+}$	2.70	2.60	∼ 2.0	>2.0	3.7×10^{8}	3.8×10^{8}

[a] Measured by single-photon counting technique. [b] Measured by ultrafast transient absorption spectroscopy. [c] Estimated from the prompt formation of the 520 nm absorption; see Discussion. [d] obtained from the rise of the 520 nm absorption; see Discussion. [e] Calculated as the reciprocal of the lifetimes obtained in transient absorption (n = 1, 2) or emission (n = 3−5) measurements.

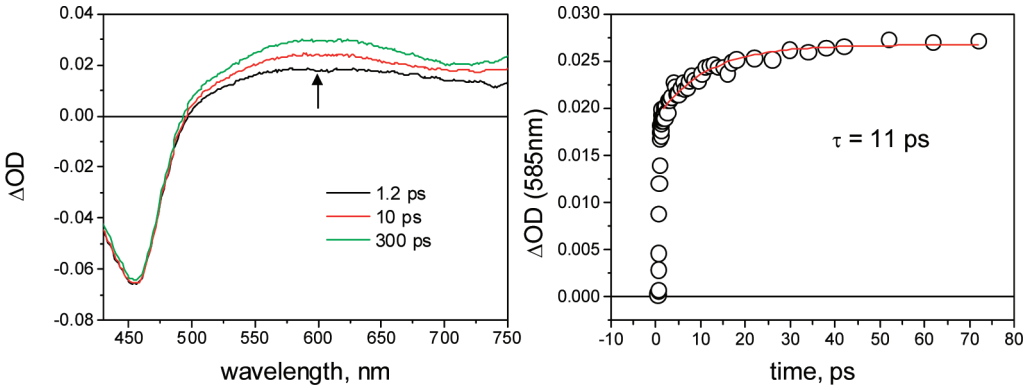

Figure 4. Ultrafast spectroscopy of the $Ru(bpy)_2(bpy-ph-bpy)^{2+}$ model in acetonitrile.

of the dyads. Upon reduction of the DQ^{2+} unit, besides the expected increase in absorbance at 387 nm and at λ > 490 nm,[20] the disappearance of the intense bands in the 350−450 nm region, characteristic of the dyads with n = 2−5, was observed. Spectroelectrochemical results for $Ru(bpy)_2(bpy-ph-DQ)^{4+}$ and $Ru(bpy)_2(bpy-ph_4-DQ)^{4+}$ are reported as an example in Figure S2 of the Supporting Information.

Emission Measurements. At room temperature, for all the dyads studied, the long-lived ^{3}MLCT emission typical of the ruthenium(II) polypyridine complexes is very efficiently (>99%) quenched relative to that observed for the corresponding nonquaternarized $Ru(bpy)_2(bpy-ph_n-bpy)^{2+}$ models (practically independent of n, Φ = 0.01, τ = 220 ns, aerated CH_3CN solution). The emission lifetimes were measured in CH_3CN and CH_2Cl_2 solutions by single-photon counting technique. For the dyads with n = 3−5 in CH_3CN and n = 2−5 in CH_2Cl_2, the decays observed are always monoexponential[21] with lifetimes (Table 2) remarkably shorter with respect to those of the nonquaternarized models. The decay for $Ru(bpy)_2(bpy-ph_3-DQ)^{4+}$ in CH_3CN is presented in Figure S3 as an example. In the case of the dyads with n = 1 and n = 2 in CH_3CN and with n = 1 in CH_2Cl_2, the lifetime is shorter than the time resolution of the instrument used (ca. 250 ps).

Transient Absorption Measurements. All the dyads were investigated by ultrafast time-resolved absorption spectroscopy (λ_{exc} = 400 nm) in CH_3CN and in CH_2Cl_2. For comparison, experiments were also performed for the nonquaternarized models under the same experimental conditions.

$Ru(bpy)_2(bpy-ph-DQ)^{4+}$. The transient behavior observed upon 400 nm excitation of CH_3CN solutions of the $Ru(bpy)_2(bpy-ph-bpy)^{2+}$ model is summarized in Figure 4. The transient spectrum is characterized by a ground-state bleach around 450 nm and a broad positive absorption at λ > 500 nm. While the instantaneous (<1 ps) bleach of the ground-state absorption at 450 nm remains constant over the whole kinetic range of the experiment (1−1000 ps), the positive absorption, after the initial instantaneous rise (<1 ps), undergoes a further increase with a time constant of ca. 11 ps (Figure 4). On a longer time scale, this absorption remains constant over the time window of the instrument.

The ultrafast results obtained for quaternarized dyad $Ru(bpy)_2(bpy-ph-DQ)^{4+}$ in CH_3CN are depicted in Figure 5. The behavior observed is significantly different from that of the $Ru(bpy)_2(bpy-ph-bpy)^{2+}$ model in the same solvent. The initial spectrum, taken immediately after the excitation pulse (t = 1 ps), exhibits, besides a bleach of the ground-state absorption at 450 nm and a broad positive absorption at λ > 550 nm, a sharp absorption maximum at 515 nm (Figure 5a). The transient spectral changes are biphasic, with a first fast process with time constant of 3.7 ps (Figure 5b), in which the 515 nm maximum disappears and the 450 nm bleach undergoes a partial (ca. one-third) recovery, while the broad absorption at λ > 550 nm remains constant. The subsequent spectral changes (7−120 ps) exhibit a clean decay to the baseline (Figure 5c), with a time constant of 18 ps (Figure 5d).

Ultrafast results obtained in CH_2Cl_2 (Figure 6) clearly indicate that the polarity of solvent has a strong effect on the kinetics of the transient spectral changes. The features of the transient spectrum (a bleach at 450 nm, a broad positive absorption at λ > 550 nm, and a sharp absorption maximum at 520 nm) are qualitatively very similar to those observed in CH_3CN, but in this solvent the formation of the positive absorption maximum at 520 nm is time-resolved (Figure 6a). This formation is biphasic

dx.doi.org/10.1021/jp209858p |J. Phys. Chem. A 2012, 116, 119–131

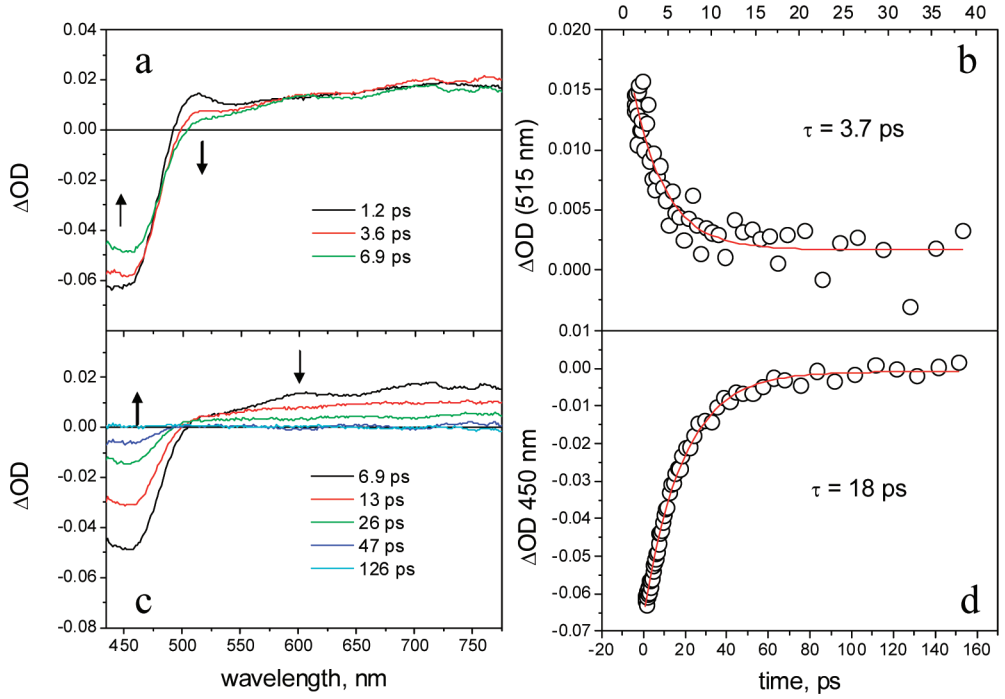

Figure 5. Ultrafast spectroscopy of the $Ru(bpy)_2(bpy-ph-DQ)^{4+}$ dyad in CH_3CN.

(Figure 6b) with an ultrafast component (ca. 30%, time constant of ca. 2 ps) and a slower component (ca. 70%, time constant of 15 ps). In this early time scale, the bleach and the broad absorption remain almost constant. In the longer time scale (23−800 ps, Figure 6c), the transient spectrum decays cleanly to the baseline. A value of 190 ps for the time constant is obtained by kinetic analysis of the bleach at 455 nm as well as of the absorption at 510 nm (Figure 6d).

$Ru(bpy)_2(bpy-ph_n-DQ)^{4+}$ (n = 2−5). In ultrafast spectroscopy, the qualitative behavior of the $Ru(bpy)_2(bpy-ph_n-DQ)^{4+}$ dyads with n = 2−5 is rather homogeneous within the series. The decay for $Ru(bpy)_2(bpy-ph_3-DQ)^{4+}$ (in CH_3CN, 400 nm excitation wavelength) is reported as an example in Figure 7. The transient spectrum observed after a few picoseconds[22] is the same observed for the respective nonquaternarized model compounds (see, e.g., Figure S4 of the Supporting Information), i.e., the typical spectrum of the MLCT excited state with a bleach at 450 nm and a broad absorption at λ > 550 nm. This transient spectrum decays cleanly to the ground state (isosbestic points at ΔOD = 0) with a time constant dependent on the number of phenyl units of the bridge. The lifetimes obtained by kinetic analysis are sensitive to solvent and span a wide range of values (Table 2). The values for n = 3, 4 in CH_3CN and for n = 3, 4, 5 in CH_2Cl_2, too long for an accurate measurement in the time window of the experiment, are only approximate estimates. No transient absorption signals can be observed in nanosecond flash photolysis experiments on the same systems (355 nm excitation, time resolution ≥ 8 ns).

Computational Results. Gas-phase ground-state optimized geometries have been calculated for the $Ru(bpy)_2(bpy-ph_n-DQ)^{4+}$ dyads with n = 1−4. In all cases, donor/bridge dihedral angles have been calculated at ca. 30°, while phenylene/phenylene dihedral angles lie in the range between 28 and 35° and bridge/acceptor dihedral angles are ca. 17°. These values are relevant to the electronic couplings along the modular bridge and between components. Molecular orbitals and their relative energies have been calculated in gas phase and CH_3CN for n = 1−4 (Figures S6−S10 of the Supporting Information) and also in CH_2Cl_2 for n = 4. Introducing solvent via the polarizable continuum model increases the HOMO−LUMO gap (CH_3CN > CH_2Cl_2 > gas phase) but does not alter the orbital relative positioning on an energy scale. Gas-phase geometry optimization of the lowest triplet state for n = 4 gives a structure where donor/bridge dihedral angle is 32°, phenylene/phenylene dihedral angles lie in the range between 20 and 28°, and the bridge/acceptor dihedral angle is 27°. Singly occupied orbitals calculated for n = 4 in gas phase, CH_2Cl_2, and CH_3CN, are found to be bridge-localized and DQ-localized. The resulting spin density is confined to the bridge−DQ region (Figure S11 of the Supporting Information). Some relevant computational results are recalled below in the Discussion Section.

DISCUSSION

Absorption Spectra. The absorption spectra of related model systems, such as the nonquaternarized analogues $Ru(bpy)_2(bpy-ph_n-bpy)^{2+}$ (Figure 2b) or the homobinuclear complexes $Ru(bpy)_2(bpy-ph_n-bpy)Ru(bpy)_2^{4+}$,[23] are a simple superposition of the ligand-centered (LC) bands (at ca. 290 nm), the metal-to-ligand charge-transfer (MLCT) bands of the ruthenium polypyridine units (at ca. 460 nm), and the $\pi-\pi^*$ bands of the oligophenylene bridge (at 320−350 nm, depending on n). The spectra of the $Ru(bpy)_2(bpy-ph_n-DQ)^{4+}$ dyads, however, in addition to the above-mentioned types of bands, display a set of new bands in the 350−450 nm range (Figure 2a) that cannot be attributed to any of the molecular components.[24] These bands are solvatochromic (Figure 3) and disappear upon electrochemical reduction of the DQ unit (Figure S2 of the Supporting Information). Thus, it is reasonable to assign them to some kind of charge-transfer transitions involving the DQ unit as acceptor. Deeper insight into the nature of such transitions can be obtained

dx.doi.org/10.1021/jp209858p |J. Phys. Chem. A 2012, 116, 119–131

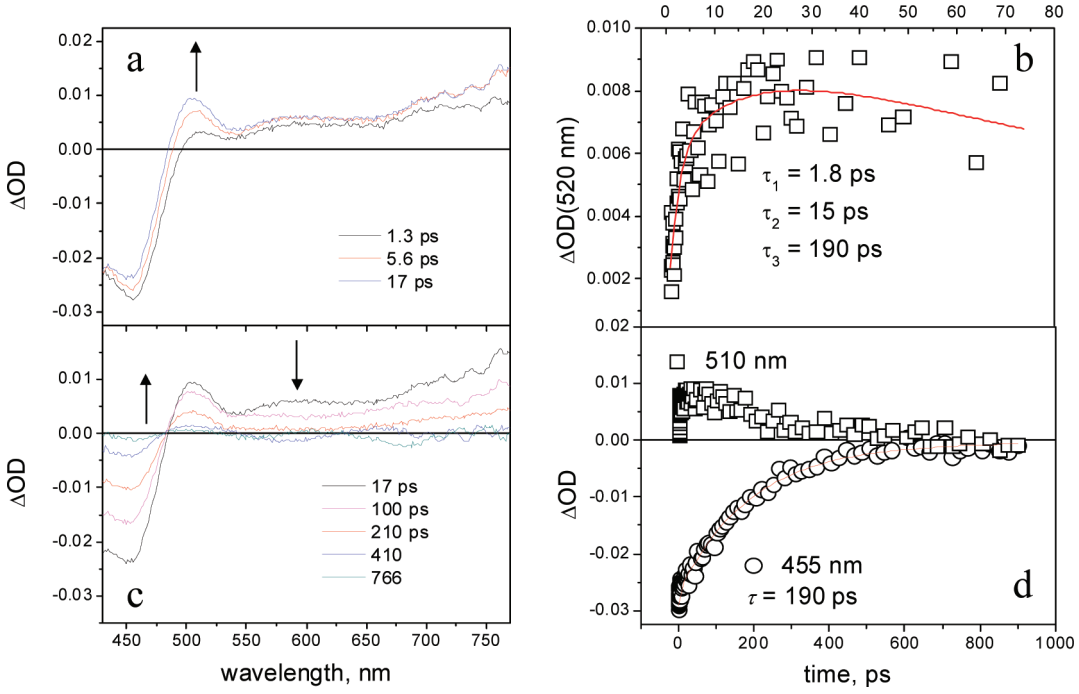

Figure 6. Ultrafast spectroscopy of the $Ru(bpy)_2(bpy-ph-DQ)^{4+}$ dyad in CH_2Cl_2.

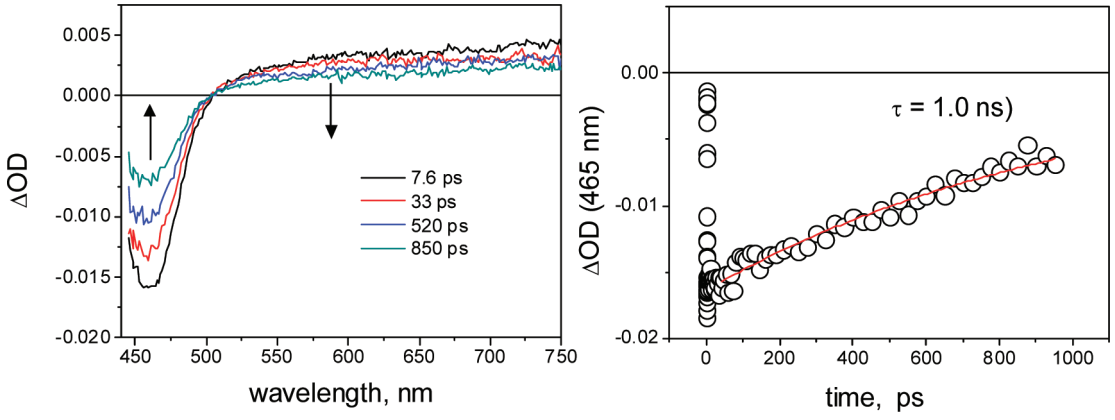

Figure 7. Ultrafast spectroscopy of the $Ru(bpy)_2(bpy-ph_3-DQ)^{4+}$ dyad in acetonitrile.

from the DFT calculations performed on this series of dyads. Some relevant orbitals of $Ru(bpy)_2(bpy-ph_2-DQ)^{4+}$ and $Ru(bpy)_2(bpy-ph_4-DQ)^{4+}$, labeled according to their predominant localization, are shown as an example in Figure 8.[25] The figure also shows how the energy of these orbitals changes along the $n = 2-4$ series. It is seen that, while the filled metal d-orbital and the vacant orbitals localized on the bipyridine fragment of the bridging ligand or on the DQ acceptor unit remain appreciably constant along the series, the highest filled orbital localized on the bridge undergoes a steady increase in energy with increasing n value. In fact, the filled bridge orbital crosses the metal d-orbital and becomes the HOMO for $n \geq 3$. Although one-electron orbital energy differences cannot simply be translated into spectroscopic excitation energies, it is evident that charge-transfer transitions having the DQ unit as the acceptor and the oligophenylene bridge as the donor are expected to occur at low energies in these systems. Taking place between MOs localized on adjacent fragments with good overlap (which is not the case, e.g., when the orbitals are localized on Ru and DQ), such charge-transfer transitions are also expected to have high oscillator strength. Thus, we assign the new bands in the 350−450 nm range of the absorption spectra of the $Ru(bpy)_2(bpy-ph_n-DQ)^{4+}$ dyads (Figure 2a) as $\pi(ph_n) \rightarrow \pi^*(DQ)$, *bridge-to-acceptor CT transitions*.

Photophysical Behavior. A typical energy level scheme for the $Ru(bpy)_2(bpy-ph_n-DQ)^{4+}$ dyads, as obtained from spectroscopic[26,23] and electrochemical data (Table 1)[27,28] in acetonitrile, is shown in Figure 9. This diagram holds with minor variations for all the complexes in the series, showing that electron transfer from the MLCT excited states of the Ru complex donor unit to the appended DQ^{2+} acceptor is thermodynamically favored by 0.33 ± 0.02 eV. Therefore, a conventional electron-transfer quenching scheme, with moderately exergonic charge separation followed by strongly exergonic charge recombination,[29] is expected to be effective in these systems. The following discussion will show that

dx.doi.org/10.1021/jp209858p | J. Phys. Chem. A 2012, 116, 119–131

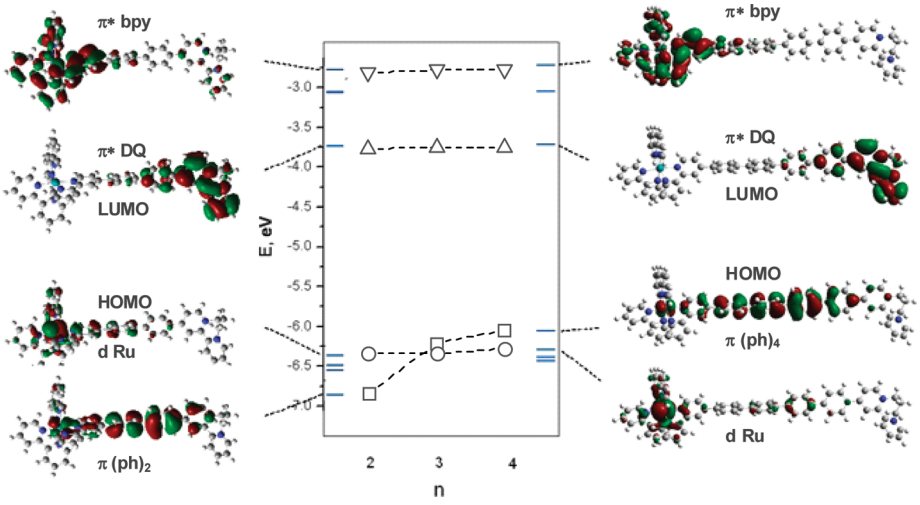

Figure 8. Relevant molecular orbitals of the $Ru(bpy)_2(bpy-ph_n-DQ)^{4+}$ dyads (n = 2, 3, 4) (for a more complete series, see the Supporting Information). The central diagram shows the energy changes undergone by orbitals with the same predominant localization along the n = 2−4 series.

the situation can be more complex than suggested by the simple scheme of Figure 9.

Since the qualitative behavior of the $Ru(bpy)_2(bpy-ph_n-DQ)^{4+}$ dyad with n = 1 is clearly different from that of the other members of the series (n = 2−5), the photophysics of these two classes of systems will be discussed separately.

$Ru(bpy)_2(bpy-ph-DQ)^{4+}$. In order to discuss the photophysics of this dyad, a comparison with the behavior of the nonquaternarized model system $Ru(bpy)_2(bpy-ph-bpy)^{2+}$ is valuable.

For the $Ru(bpy)_2(bpy-ph-bpy)^{2+}$ model, the emission energy and lifetime (626 nm and 220 ns, in aerated acetonitrile) are quite typical of Ru(II) polypyridine complexes. The slight (ca. 10 nm) red shift relative to the standard $Ru(bpy)_3^{2+}$ complex indicates that, as in related systems,[16] the emitting MLCT excited state is on the phenyl-substituted bipyridine ligand, lying at slightly lower energy than those localized on the unsubstituted bipyridines. The behavior in ultrafast time-resolved spectroscopy, however, is significantly different from that of $Ru(bpy)_3^{2+}$. In particular (Figure 4), while the instantaneous bleach of the ground-state MLCT band at 450 nm remains constant over the 1−1000 ps time range, the positive ligand radical anion absorption in the λ > 500 nm range, after the initial instantaneous rise, undergoes a further increase with time constant of 11 ps. As shown by previous nanosecond work,[23] complexes of phenyl-substituted bipyridine exhibit larger transient absorption in this spectral range than the simple $Ru(bpy)_3^{2+}$ complex. Therefore, the biphasic increase observed here can be attributed to MLCT excitation followed by the relaxation of states involving the bpy ligands to the lowest state involving the phenyl-substituted bipyridine and provides a direct spectroscopic measurement of the rate of interligand electron transfer (ILET) in the complex. A time constant of 47 ps was estimated for ILET in $Ru(bpy)_3^{2+}$ in acetonitrile by Malone and Kelley[30] using time-resolved absorption polarization spectroscopy. Subsequently, with a better instrumental resolution, Papanikolas and co-workers[31] measured a lifetime of 8.7 ps for ILET in $Os(bpy)_3^{2+}$. The time constant, 11 ps, obtained here for $Ru(bpy)_2(bpy-ph-bpy)^{2+}$ is close to this last figure.[32]

In $Ru(bpy)_2(bpy-ph-DQ)^{4+}$, the MLCT emission is very efficiently (>99%) quenched relative to the model compound, with an emission lifetime shorter than the time resolution of the single-photon counting instrument used (Table 2). The behavior

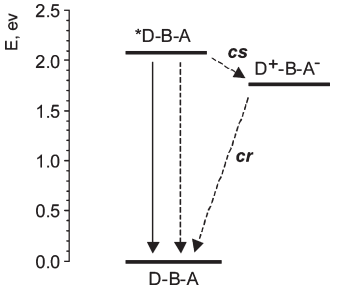

Figure 9. General energy level diagram for the $Ru(bpy)_2(bpy-ph_n-DQ)^{4+}$ dyads, where D = $Ru(bpy)_2bpy^{2+}$, B = $-ph_n-$, and A = $-DQ^{2+}$.

observed in ultrafast spectroscopy (Figures 5 and 6) is complex and solvent-dependent and deserves a careful examination.

In CH_3CN, the initial spectrum (1.2 ps in Figure 5) is clearly different from that of the $Ru(bpy)_2(bpy-ph-bpy)^{2+}$ model (Figure 4), featuring, besides the usual bleach of the ground-state absorption at 450 nm and the broad positive absorption at λ > 550 nm, also a sharp maximum at 515 nm. This maximum is characteristic of the reduced form of the DQ acceptor (λ = 514 nm, ε = 4.400 M^{-1} cm^{-1}),[33] suggesting that intramolecular electron transfer with formation of Ru(III) and reduced DQ^{2+} takes place promptly, i.e., in the subpicosecond time domain. As this time scale is much shorter than that for interligand electron hopping (11 ps in the $Ru(bpy)_2(bpy-ph-bpy)^{2+}$ model, see above), the prompt electron-transfer quenching is likely to involve only about one-third of the MLCT states, i. e., those localized on the quencher-functionalized bipyridine. Thus, in the initial transient spectrum, the 450 nm bleach can be attributed by ca. one-third to the charge-separated state and by ca. two-thirds to the MLCT states localized on the outer bipyridine ligands. The subsequent transient spectral changes are biphasic, with a first fast process, with time constant of 3.7 ps, in which the 515 nm maximum disappears, the 450 nm bleach undergoes a partial (ca. one-third) recovery, and the broad absorption at λ > 550 nm remains constant. This behavior is exactly as expected for charge recombination of the electron-transfer state, considering that the various MLCT states do not interconvert in this time scale. The final spectrum of this step (6.9 ps in Figure 5) is thus a

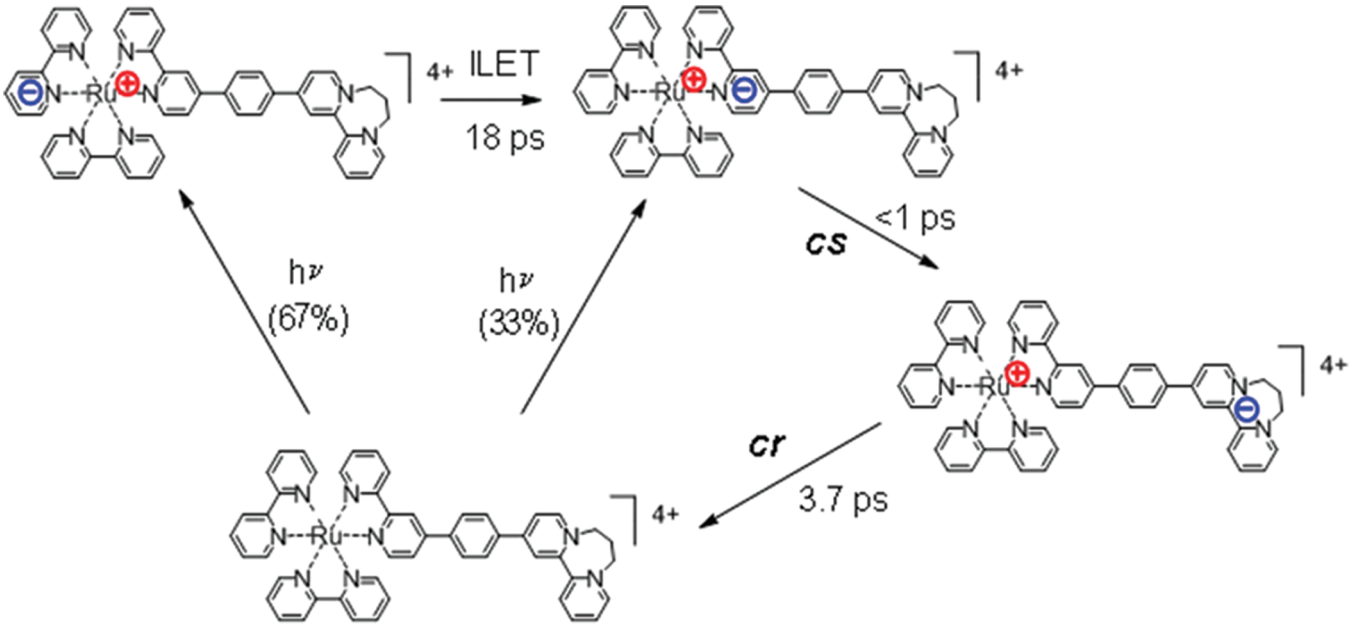

Figure 10. Schematic representation of the electron-transfer processes involved in the photophysical mechanism for $Ru(bpy)_2(bpy-ph-DQ)^{4+}$ in CH_3CN.

typical MLCT excited-state spectrum, representing the MLCT states localized on the outer bipyridine ligands. The subsequent decay of the spectral changes leads cleanly to the baseline, with time constant of 18 ps. Since this figure is close to that for interligand hopping,[34] it seems likely to associate this process to a rate-limiting conversion of the MLCT states localized on the outer bipyridine ligands to that localized on the quencher-functionalized one, followed by fast electron transfer and charge recombination to the ground state. The photophysical mechanism is sketched in Figure 10.

When the solvent is changed from CH_3CN to CH_2Cl_2, the energy of the charge-separated state is expected to increase (by ca. 0.1 eV, from Weller-type[28] calculation) and the reorganizational energy to decrease. This has important consequences in the time-resolved spectroscopic behavior (Figure 6). The decrease in driving force, only partially compensated (in the Marcus normal region) by the lower reorganizational energy, makes now the charge separation step somewhat slower. The consequence is that the formation of the 520 nm maximum characteristic of the reduced DQ unit is now time-resolved, with a fast component (1.8 ps) assigned to direct charge separation (electron transfer within the quencher-functionalized bipyridine) and a slower component (ca. 15 ps) assigned to ILET from the outer bipyridines. In CH_2Cl_2, the charge recombination process, which lies in the Marcus inverted region, undergoes a strong decrease in rate (190 ps), under the combined effects of the increase in driving force and decrease in reorganizational energy. As this process is now much slower than both direct charge separation and ILET, in time-resolved spectroscopy the charge-separated state first accumulates and then undergoes a clean decay to the baseline. The kinetic differences between acetonitrile and dichloromethane are summarized in Figure 11.

The very fast rate observed for charge separation (<1 ps) in $Ru(bpy)_2(bpy-ph-DQ)^{4+}$ suggests that the donor−acceptor electronic coupling is relatively strong through this short bridge. This is in line with the results of DFT calculations, which show that the phenyl spacer is only slightly twisted relative to the adjacent pyridyl ring of DQ, so that (Figure 12) the π^* DQ acceptor orbitals (LUMO and LUMO+1) have large amplitudes at the phenyl spacer and undergo significant direct overlap with the π^* bpy excited-state donor orbital (LUMO+2). The fact that charge separation is always faster than charge recombination likely reflects a combination of nuclear (normal vs inverted Marcus region) and electronic factors (less efficient coupling for charge recombination, involving π^* DQ LUMO and d Ru HOMO).

$Ru(bpy)_2(bpy-ph_n-DQ)^{4+}$ (n = 2−5). The behavior of the $Ru(bpy)_2(bpy-ph_n-DQ)^{4+}$ dyads with $n = 2-5$ is qualitatively rather homogeneous. The emission intensity and lifetime are always strongly (>99%) quenched relative to those of the respective nonquaternarized model compounds. The transient spectral changes obtained by ultrafast spectroscopy (after a short, ca. 10 ps, delay)[22,35] apparently exhibit a clean decay of the typical triplet MLCT excited-state spectrum down to the ground state. Where both measurements are feasible (i.e., for $n = 3$ in CH_3CN and $n = 2$ in CH_2Cl_2), the lifetimes obtained from emission decay and transient spectroscopy are comparable (Table 2). Thus, the overall picture is that of a series of dyads in which a rate-determining quenching step is followed by faster processes leading to the ground state, without accumulation of intermediate transient products. Within this general qualitative behavior, the $n = 2-5$ systems differ in kinetics, spanning a wide range of lifetimes.

In an electron-transfer quenching mechanism (holding true for this series of dyads with the possible exception, see below, of $n = 4, 5$), the observed behavior implies a change in kinetic regime from $n = 1$ (charge separation faster than charge recombination) to $n \geq 2$ (charge recombination faster than charge separation). The reasons can be discussed in terms of electron-transfer theory. As the energetics (MLCT energy and redox potentials) are virtually the same for the two systems, the nuclear factors (FCWD in eq 1) for charge separation and recombination are also expected to be practically the same for $n = 1$ and $n = 2$.[36] Therefore, the reasons for the change in kinetic regime must be sought in the electronic factors. For $n = 1$, we have already remarked

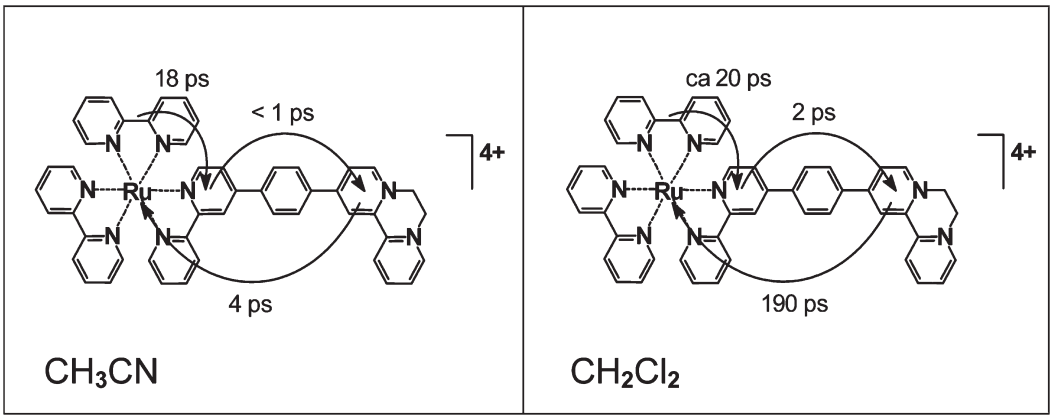

Figure 11. Schematic summary of the kinetic behavior of $Ru(bpy)_2(bpy-ph-DQ)^{4+}$ in acetonitrile and dichloromethane.

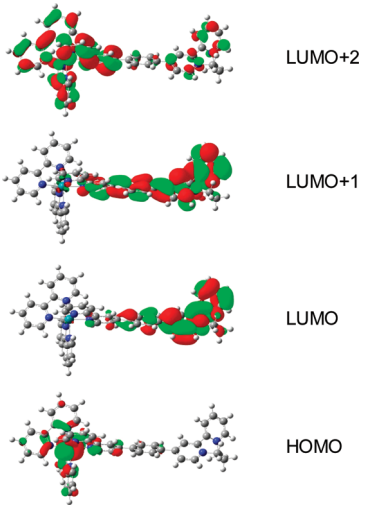

Figure 12. Frontier molecular orbitals of $Ru(bpy)_2(bpy-ph-DQ)^{4+}$.

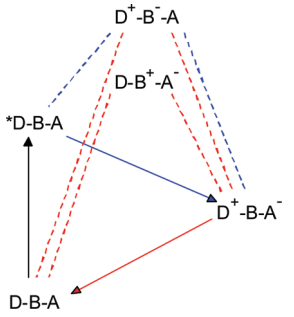

Figure 13. Schematic representation of the superexchange pathways available to photoinduced charge separation (cs, blue) and charge recombination (cr, red).

that the very fast charge separation can be related to the efficient overlap between the donor and acceptor orbitals, which provides strong direct donor−acceptor electronic coupling. In this case, second-order interaction via virtual states can be disregarded.[37] For $n \geq 2$, on the other hand, direct overlap is much less efficient (Figure 8 and Figures S7−S10 of the Supporting Information), and a superexchange mechanism (eq 2) is appropriate to describe the donor−acceptor electronic couplings. In general terms (Figure 1), both electron- and hole-transfer virtual states involving the bridge can be considered as superexchange mediators. When electron transfer is photochemically induced, however, different superexchange mechanisms apply to charge separation and recombination. When excitation takes place at the donor (Figure 13), both electron- and hole-transfer virtual states can in principle mediate charge recombination, but only the electron-transfer virtual state can affect charge separation (the D*−B−A excited state and the $D-B^+-A^-$ hole-transfer state differ by a two-electron shift and cannot mix effectively). Thus, for charge separation only the first term of eq 2 should be retained, while for charge recombination both terms could in principle operate. In practice, for oligophenylene bridges, the electron-transfer virtual states lie at much higher energy than the hole-transfer ones (Table 3), so that only the hole-transfer superexchange pathway is expected to dominate charge recombination. The energy gaps with the appropriate virtual states estimated[38] for the two pathways (Table 3) clearly show that, in terms of the denominators in eq 2, charge recombination is highly favored over charge separation. Of course, electronic coupling is not the only factor determining the rates (eq 1). The experimental evidence that no accumulation of the charge-separated state takes place, however, seems to indicate that in these systems the effect of the nuclear factors (which, per se, would favor charge separation) is overcome by that of the superexchange electronic factors.

As discussed above, the rate constants for $n \geq 2$ reflect the primary quenching step that leads to disappearance of the MLCT excited state. When these rate constants are plotted against n (Figure 14), however, the behavior is quite different from the regular exponential decay expected on the basis of simple theory (eq 4) and found in several studies of distance dependence of electron transfer.[3] We suggest that the main reason for the nonideal behavior of this series of dyads lies in the breakdown of the main assumption embedded in eq 2, i.e., that the energy of the virtual charge-transfer states involving the bridge is essentially constant. In fact, as inferred from Table 3, these states are expected to undergo quite substantial energy changes along the series. Besides being responsible, as discussed above, for the fast charge recombination occurring in these systems, the presence of low-lying bridge-localized charge-transfer states is likely to have a deep effect also on the trend observed for $n = 2-5$. The main point is that, as the bridge is elongated, charge-transfer states involving the bridge may become sufficiently low in energy as to have an active, direct role in the quenching of the excited state.

A rough idea of the relative energy orderings of the relevant electronic states in the $n = 2-4$ series can be obtained from the

Table 3. Redox Properties of Oligo-*p*-phenylenes and Estimated Energies of the Electron- and Hole-Transfer States in the $Ru(bpy)_2(bpy-ph_n-DQ)^{4+}$ Dyads

			$Ru(bpy)_2(bpy-ph_n-DQ)^{4+}$ = D−B−A			
	ph_n		[$Ru(bpy)_2bpy-$ = D, ph_n = B, $-DQ$ = A]			
n	E_{ox} [a,b](V)	E_{red} [a,c](V)	$E(D-B^+-A^-)$ (eV)[d]	$E(D^+-B^--A)$ (eV)[d]	$\Delta E(h^+)cs$ [d,e]	$\Delta E(e^-)cs$ [d,f]
2	1.81	−2.72	2.33	4.01	0.53	1.93
3	1.56	−2.44	2.08	3.73	0.28	1.65
4	1.43	−2.32	1.95	3.61	0.15	1.53
5	1.36[g]	−2.24[g]	1.88	3.53	0.08	1.45

[a] Versus SCE, adapted from Meerholz, K; Heinze, J. *Electrochimica Acta* **1996**, *41*, 1839. [b] Dichloromethane. [c] Dmethylamine. [d] Neglecting electrostatic work term corrections. [e] $\Delta E(e^-)cs = E(D-B^+-A^-) - E(^*D-B-A)$. [f] $\Delta E(h^+)cs = E(D^+-B^--A) - E(D^+-B-A^-)$. [g] Estimated from data for $(ph)_1-(ph)_4$ and $(ph)_6$.

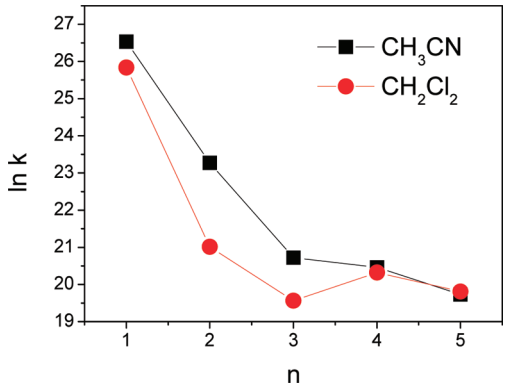

Figure 14. Logarithmic plot of the rate constants for excited-state decay as a function of the number of spacers in the bridge.

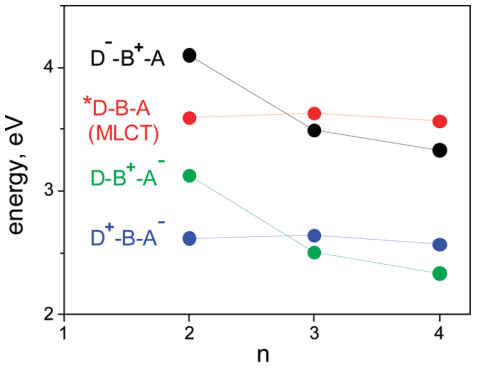

Figure 15. Approximate energy ordering of the various types of excited states in $Ru(bpy)_2(bpy-ph_n-DQ)^{4+}$ dyads (n = 2−5), as obtained from MO energy differences.

orbital energies in Figure 15. As already noticed, the filled bridge orbital undergoes a steady increase in energy along the series and, at ca. n = 3, raises above the metal-centered orbitals, becoming the HOMO. In an admittedly very crude approximation, where relative excited-state energies are estimated from MO energy differences (Figure 8), it is predicted that at ca. n = 3 two relevant state crossings may occur: (i) charge-transfer states of bridge-to−bpy type (D^-B^+A) may become comparable or lower in energy than the MLCT excited state, and (ii) the lowest excited state of the dyads switches from charge-separated state (D^+B-A^-) to bridge-to-DQ charge-transfer state (DB^+A^-).[39] From this viewpoint, it is no wonder that the decrease in quenching rate (elongation in lifetimes) of the MLCT state does not follow the standard exponential behavior. In particular from point (i), the abrupt stop taking place around n = 3 can be most likely attributed to a change in quenching mechanism: from π^*(bpy) → π^*(DQ) electron transfer ($^*D-B-A \rightarrow D^+-B-A^-$) to π(bridge) → d(Ru) electron transfer ($^*D-B-A \rightarrow D^-B^+A$). As to the presence of low-lying states of the DB^+A^- type, they are probably of little relevance to the decay of the MLCT excited state, since a $^*D-B-A \rightarrow DB^+A^-$ process, though thermodynamically allowed (Figure 15), would involve two simultaneous electron-transfer steps: π^*(bpy) → π^*(DQ), π(bridge) → d(Ru.). Such type of states can, on the other hand, be very efficient mediators of the D^+-B-A^- → D−B−A charge recombination, either as superexchange hole-transfer virtual states (Figure 13) or, perhaps, for the longer dyads (point ii), even as real intermediate states.

CONCLUSIONS

The main conclusions of this work can be summarized as follows:

(i) In the $Ru(bpy)_2(bpy-ph_n-DQ)^{4+}$ dyads, new spectroscopic transitions are observed, in addition to those characteristic of the donor, bridge, and acceptor fragments. DFT calculations point out the presence of filled bridge-localized orbitals at high energy and suggest the assignment of such bands as bridge-to-acceptor (π ph_n) → (π^* DQ) charge-transfer transitions.

(ii) The $Ru(bpy)_2(bpy-ph-DQ)^{4+}$ dyad (n = 1) undergoes very fast (few picosecond) photoinduced electron transfer followed by slower charge recombination. The ultrafast charge separation is a consequence of good overlap between the π^* bpy and π^* DQ orbitals, which provides good, direct donor−acceptor electronic coupling. The ultrafast electron-transfer step takes place from the MLCT state localized on the functionalized ligand and is time-resolved with respect to the slower interligand hopping processes. Charge separation is kinetically favored over charge recombination by both nuclear (normal vs inverted region) and electronic (better coupling) factors.

(iii) In the $Ru(bpy)_2(bpy-ph_n-DQ)^{4+}$ dyads with n = 2−5, MLCT excited-state quenching takes place without accumulation of charge-separated product, suggesting that charge recombination is faster than charge separation. This behavior can be rationalized in terms of the superexchange

dx.doi.org/10.1021/jp209858p |*J. Phys. Chem. A* 2012, 116, 119–131

couplings for the two processes: with this type of bridges, the electron-transfer virtual states required for charge separation lie at very high energy, whereas charge recombination is efficiently mediated by low-energy virtual states of the hole-transfer type.

(iv) The kinetics of MLCT quenching in the $Ru(bpy)_2(bpy-ph_n-DQ)^{4+}$ dyads with $n = 1-5$ does not follow the usual exponential falloff with number of spacers (or distance): after a regular decrease from $n = 1$ to 3, the rate constants become almost insensitive to bridge length for $n = 3-5$. Now, $n = 3$ is precisely the dyad length at which a filled bridge-localized orbital, increasing steadily in energy along the series, replaces the Ru d-orbitals as the HOMO of the system. Thus, the uncommon kinetic behavior is rationalized by a change in quenching mechanism with increasing bridge length from oxidative quenching by the DQ acceptor to reductive quenching by the bridge.

(v) Generally speaking, oligo *p*-phenylene bridges have substantial drawbacks from the viewpoint of achieving efficient, long-lived charge separation upon donor excitation in donor−bridge-acceptor dyads. These bridges are characterized by relatively high-energy filled orbitals, and, in this type of dyads, this (a) will generally favor charge recombination via hole-transfer superexchange pathways and (b) may, for long bridges, switch on new quenching mechanisms other than electron transfer to the acceptor. The same type of bridges are expected to perform much better, on the other hand, when electron transfer in the dyad is promoted by excitation of the acceptor.[6,8,12,17] In this case, the situation is reversed, with hole-transfer superexchange pathways favoring charge separation.

■ ASSOCIATED CONTENT

Supporting Information. ^1H NMR spectrum of $Ru(bpy)_2(bpy-ph_2-DQ)^{4+}$; spectroelectrochemistry of $Ru(bpy)_2(bpy-ph-DQ)^{4+}$ and of $Ru(bpy)_2(bpy-ph_4-DQ)^{4+}$; emission decay for $Ru(bpy)_2(bpy-ph_3-DQ)^{4+}$; ultrafast spectroscopy of $Ru(bpy)_2(bpy-ph_3-bpy)^{2+}$ model; ultrafast spectroscopy of $Ru(bpy)_2(bpy-ph_2-DQ)^{4+}$ as a function of excitation wavelength, relevant MOs of $Ru(bpy)_2(bpy-ph_n-DQ)^{4+}$ ($n = 1-4$); spin density plot for the lowest triplet state of $Ru(bpy)_2(bpy-ph_4-DQ)^{4+}$. This material is available free of charge via the Internet at http://pubs.acs.org.

■ AUTHOR INFORMATION

Corresponding Author

*E-mail: snf@unife.it (F.S.); decola@uni-muenster.de (L.D.C.).

Present Addresses

[||]Chemical Technologies International s.r.l, 44100 Ferrara, Italy.

[▽]Université Joseph Fourier Grenoble 1/CNRS, Département de Chimie Moléculaire, UMR 5250, Laboratoire de Chimie Inorganique Rédox, Institut de Chimie Moléculaire de Grenoble FR-CNRS-2607, BP 53, 38041 Grenoble Cedex 9, France.

[△]European Patent Ofice, Patentlaan 2, 2288EE Rijswijk, Netherlands.

[▼]Molecular Stamping s.r.l., Fondazione Bruno Kessler, 38123 Trento, Italy.

■ ACKNOWLEDGMENT

Financial support by the EC (Grant G5RD-CT-2002-00776, MWFM) and by the Italian MIUR (PRIN 20085ZXFEE) is gratefully acknowledged.

■ REFERENCES

(1) (a) Lewis, N. S.; Nocera, D. G. *Proc. Natl. Acad. Sci. U.S.A.* **2006**, *103*, 15729–15735. (b) Wasielewski, M. R. *J. Org. Chem.* **2006**, *71*, 5051–5066. (c) Hambourger, M.; Moore, G. F.; Kramer, D. M.; Gust, D.; Moore, A. L.; Moore, T. A. *Chem. Soc. Rev.* **2009**, *38*, 25–35.

(2) (a) *Molecular Electronics*; Jortner, J., Ratner, M., Eds.; Blackwell Science: London, U.K., 1997. (b) Aviram, A; Ratner, M. A. *Ann. N.Y. Acad, Sci.* **1998**, *852* (Special Volume on Molecular Electronics). (c) Joachim, C.; Gimzewski, J. K.; Aviram, A. Electronics using hybrid-molecular and mono-molecular devices. *Nature* **2000**, *408*, 541. (d) Tour, J. M. *Acc. Chem. Res.* **2000**, *33*, 791–804. (e) Pease, A. R.; Jeppesen, J. O.; Stoddart, J. F.; Luo, Y.; Collier, C. P.; Heath, J. R. *Acc. Chem. Res.* **2001**, *34*, 433.

(3) (a) Paddon-Row, M. N. In *Electron Transfer in Chemistry*; Balzani, V., Ed.; Wiley-VCH: Weinheim, Germany, 2001; Vol. III, Chapter 2.1, p 179. (b) Scandola, F.; Chiorboli, C.; Indelli, M. T.; Rampi, M. A. In *Electron Transfer in Chemistry*; Balzani, V., Ed.; Wiley-VCH: Weinheim, Germany, 2001; Vol. III, Chapter 2.3, p 337. (c) Petersson, K.; Wiberg, J.; Ljungdahl, T.; Martensson, J.; Albinsson, B *J. Phys. Chem. A* **2006**, *110*, 319. (d) Albinsson, B.; Mårtensson, J. *J. Photochem. Photobiol., C* **2008**, *9*, 138–155.

(4) (a) Marcus, R. A. *Annu. Rev. Phys. Chem.* **1964**, *15*, 155. (b) Sutin, N. *Prog. Inorg. Chem.* **1983**, *30*, 441. (c) Miller, J. R.; Beitz, J. V.; Huddleston, R. K. *J. Am. Chem. Soc.* **1984**, *106*, 5057. (d) Marcus, R. A.; Sutin, N. *Biochim. Biophys. Acta* **1985**, *811*, 265. (e) Jortner, J. *J. Chem. Phys.* **1976**, *64*, 4860. (f) Bixon, M.; Jortner, J. *Adv. Chem. Phys.* **1999**, *106*, 35. (g) Newton, M. D. *Chem. Rev.* **1991**, *91*, 767.

(5) (a) Halpern, J.; Orgel, L. E. *Discuss. Faraday Soc.* **1960**, *29*, 32. (b) McConnell, H. M. *J. Chem. Phys.* **1961**, *35*, 508. (c) Mayoh, B.; Day, P. *J. Chem. Soc., Dalton Trans.* **1974**, 846. (d) Miller, J. R.; Beitz, J. V. *J. Chem. Phys.* **1981**, *74*, 6746. (e) Richardson, D. E.; Taube, H. *J. Am. Chem. Soc.* **1983**, *105*, 40.

(6) For a clear demonstration of such a dependence, see, e.g.: (a) Hanss, D.; Wenger, O. S. *Inorg. Chem.* **2008**, *47*, 9081–9084. (b) Hanss, D.; Wenger, O. S. *Inorg. Chem.* **2009**, *48*, 671–680.

(7) Davis, W. B.; Svec, W. A.; Ratner, M. A.; Wasielewski, M. R. *Nature* **1998**, *396*, 60.

(8) Weiss, E. A.; Ahrens, M. J.; Sinks, L. E.; Ratner, M. A.; Wasielewski, M. R. *J. Am. Chem. Soc.* **2004**, *126*, 5577.

(9) Zojer, E.; Cornil, J.; Leising, G.; Brédas, J. L. *Phys. Rev. B* **1999**, *59*, 7957.

(10) Onuchic, J. N.; Beratan, D. N. *J. Am. Chem. Soc.* **1987**, *109*, 6771.

(11) (a) Helms, A.; Heiler, D.; McLendon, G. J. *Am. Chem. Soc.* **1991**, *113*, 4325. (b) Helms, A.; Heiler, D.; McLendon, G. J. *Am. Chem. Soc.* **1992**, *114*, 6227.

(12) (a) Weiss, E. A.; Ahrens, M. J.; Sinks, L. E.; Ratner, M. A.; Wasielewski, M. A. *J. Am. Chem. Soc.* **2004**, *126*, 9510. (b) Weiss, E. A.; Tauber, M. J.; Kelley, R. F.; Ahrens, M. J.; Ratner, M. A.; Wasielewski, M. R. *J. Am. Chem. Soc.* **2005**, *127*, 11842.

(13) (a) Barigelletti, F.; Flamigni, L.; Guardigli, M.; Juris, A.; Beley, M.; Chodorowski-Kimmes, S.; Collin, J.-P.; Sauvage, J.-P. *Inorg. Chem.* **1996**, *35*, 136. (b) Barigelletti, F.; Flamigni, L.; Collin, J.-P.; Sauvage, J.-P. *Chem. Commun.* **1997**, 333. (c) Collin, J.-P.; Gavina, P.; Heitz, V.; Sauvage, J.-P. *Eur. J. Inorg. Chem.* **1998**, 1.

(14) (a) Schlicke, B.; Belser, P.; De Cola, L.; Sabbioni, E.; Balzani, B. *J. Am. Chem. Soc.* **1999**, *121*, 4207.(b) De Cola, L.; Belser, P. In *Electron Transfer in Chemistry*; Balzani, V., Ed.; Wiley-VCH, Verlag GmbH: Weinheim, Germany, 2001; Vol. 5, p 97. (c) Welter, S.; Salluce, N.; Belser, P.; Groeneveld, M.; De Cola, L. *Coord. Chem. Rev.* **2005**, *249*, 1360.

(15) Welter, S.; Lafolet, F.; Cecchetto, E.; Vergeer, F.; De Cola, L. *Chem. Phys. Chem.* **2005**, *6*, 2417.
(16) Indelli, M. T.; Chiorboli, C.; Flamigni, L.; De Cola, L.; Scandola, F. *Inorg. Chem.* **2007**, *46*, 5630–5641.
(17) Wenger, O. *Acc. Chem. Res.* **2011**, *44*, 25–35.
(18) Chiorboli, C.; Rodgers, M. A. J.; Scandola, F. *J. Am. Chem. Soc.* **2003**, *125*, 483.
(19) Frisch, M. J.; Trucks, G. W.; Schlegel, H. B.; Scuseria, G. E.; Robb, M. A.; Cheeseman, J. R.; Montgomery, J. A., Jr.; Vreven, T.; Kudin, K. N.; Burant, J. C.; Millam, J. M.; Iyengar, S. S.; Tomasi, J.; Barone, V.; Mennucci, B.; Cossi, M.; Scalmani, G.; Rega, N.; Petersson, G. A.; Nakatsuji, H.; Hada, M.; Ehara, M.; Toyota, K.; Fukuda, R.; Hasegawa, J.; Ishida, M.; Nakajima, T.; Honda, Y.; Kitao, O.; Nakai, H.; Klene, M.; Li, X.; Knox, J. E.; Hratchian, H. P.; Cross, J. B.; Bakken, V.; Adamo, C.; Jaramillo, J.; Gomperts, R.; Stratmann, R. E.; Yazyev, O.; Austin, A. J.; Cammi, R.; Pomelli, C.; Ochterski, J. W.; Ayala, P. Y.; Morokuma, K.; Voth, G. A.; Salvador, P.; Dannenberg, J. J.; Zakrzewski, V. G.; Dapprich, S.; Daniels, A. D.; Strain, M. C.; Farkas, O.; Malick, D. K.; Rabuck, A. D.; Raghavachari, K.; Foresman, J. B.; Ortiz, J. V.; Cui, Q.; Baboul, A. G.; Clifford, S.; Cioslowski, J.; Stefanov, B. B.; Liu, G.; Liashenko, A.; Piskorz, P.; Komaromi, I.; Martin, R. L.; Fox, D. J.; Keith, T.; Al-Laham, M. A.; Peng, C. Y.; Nanayakkara, A.; Challacombe, M.; Gill, P. M. W.; Johnson, B.; Chen, W.; Wong, M. W.; Gonzalez, C.; Pople, J. A. *Gaussian 03*, revision C.02; Gaussian, Inc.: Wallingford CT, 2004.
(20) Elliott, C. M.; Freitag, R. A.; Blaney, D. D. *J. Am. Chem. Soc.* **1985**, *107*, 4647–4655.
(21) A minor (<5%) long-lived component, with lifetime identical to that of the corresponding model compound, is attributed to impurities of nonquaternarized species.
(22) The appearance of the MLCT transient is preceded by some fast spectral changes in the <10 ps time scale (Figure S5a in the Supporting Information). Such initial processes are likely related to the fact that the 400 nm pump light does not give direct MLCT excitation (as was the case for $n = 1$) but rather excitation in the new bands (Figure 2) of a different orbital origin (see Discussion). As expected in this hypothesis, the initial fast processes disappear (the formation of the MLCT transient becomes instantaneous) when the excitation is performed at 500 nm (Figure S5b in the Supporting Information).
(23) Welter, S.; Salluce, N.; Benetti, A.; Rot, N.; Belser, P.; Sonar, P.; Grimsdale, A. C.; Mu1llen, K.; Lutz, M.; Spek, A. L.; De Cola, L. *Inorg. Chem.* **2005**, *44*, 4706–4718.
(24) Quaternarized bipyridines typically absorb in the UV, with absorption maxima at wavelengths <290 nm.
(25) The orbitals depicted in Figure 8 for $Ru(bpy)_2(bpy-ph_2-DQ)^{4+}$ are HOMO−3, HOMO, LUMO, LUMO+2 (the predominant localization of the other orbitals in this energy range, see Figure S10 of the Supporting Information, is as follows: HOMO−2 and HOMO−1, d Ru; LUMO+1, π^* DQ). The orbitals depicted in Figure 8 for $Ru(bpy)_2(bpy-ph_4-DQ)^{4+}$ are HOMO−1, HOMO, LUMO, LUMO+2 (the predominant localization of the other orbitals in this energy range, see Figure S10 of Supporting Information, is as follows: HOMO−3 and HOMO−2, d Ru; LUMO+1, π^* DQ).
(26) The energy of the triplet MLCT state is obtained from the 77 K emission of the symmetric Ru(II) dyads.[23]
(27) The energy of the electron-transfer state, containing an oxidized ruthenium center and a reduced DQ^{2+} unit, is obtained from the measured redox potentials, considering the appropriate correction for the electrostatic work terms.[28]
(28) (a) Rehm, D.; Weller, A. *Ber. Bunsen-Ges. Phys. Chem.* **1969**, *73*, 834–839. (b) Weller, A. *Z. Phys. Chem.* **1982**, *133*, 93–98.
(29) The terms "charge separation" and "charge recombination" are strictly appropriate only for neutral dyads. We use them conventionally, however, to denote the forward and back electron-transfer processes.
(30) Malone, R. A.; Kelley, D. F. *J. Chem. Phys.* **1991**, *95*, 8970–8976.
(31) Shaw, G. B.; Brown, C. L.; Papanikolas, J. N. *J. Phys. Chem. A* **2002**, *106*, 1483–1495.
(32) In complexes of lower symmetry, ILET is expected to be faster because of the finite driving force of the process. For instance, going from $Os(bpy)_3^{2+}$ to a heteroleptic analogue with a driving force of ca. 0.1 eV, a reduction in lifetime from 8.7 to 1.5 ps was observed.[31] In our case, the driving force for ligand-to-ligand electron transfer is expected to be very small (ca. 0.03 eV, as estimated from electrochemical measurements[23] on related systems).
(33) (a) Elliott, C. M.; Freitag, R. A. *J. Chem. Soc., Chem. Commun.* **1985**, 156.
(34) The detailed energy levels of the various MLCT states could be somewhat different in $Ru(bpy)_2(bpy-ph-DQ)^{4+}$ and in $Ru(bpy)_2(bpy-ph-bpy)^{2+}$.
(35) The spectral changes in this initial time interval (bleaching of the MLCT absorption, decay of positive absorption at 520 nm, Figure S5a of the Supporting Information) very likely represent the relaxation from the bridge-to−DQ charge-transfer states populated by 400 nm light absorption to the MLCT triplet manifold, besides any equilibration between the MLCT states.
(36) In principle, a decrease in FCWD is expected to occur from $n = 1$ to $n = 2$, because of the distance dependence of the solvent reorganizational energy. The effect, however, is expected to be small. In fact, the effect depends on the relative weight of solvent and inner modes in the overall of reorganization. An upper limiting value of 20% can be calculated upon complete neglect of inner mode displacements.
(37) With a single *p*-phenylene spacer, the energy of the electron-transfer virtual state is expected to be so high (>4 eV) to make any superexchange contribution to charge separation negligible.
(38) Strictly speaking, the energy differences in eq 2 should be taken at the geometry where reactant and product states are isoenergetic (intersection geometry). Given the substantially exergonic nature of both processes, the energy of the reactant state can be used as a decent approximation.
(39) This prediction is confirmed by DFT calculations of the lowest triplet state for $n = 4$, where the singly occupied orbitals are bridge-localized and DQ-localized MOs, and the spin density is confined to the bridge−DQ region (Figure S11 of the Supporting Information)